*Progress In Electromagnetics Research, PIER 64, 69–80, 2006*

# FDTD ANALYSIS OF AN ANISOTROPICALLY COATED MISSILE

**Gong Z. Q.**

School of Information Science & Technology
Sun Yat-sen University
Guangzhou 510275, Guangdong, P. R. China

**Zhu G. Q.**

School of Electronic Information
Wuhan University
Wuhan 430072, Hubei, P. R. China

**Abstract**—In this paper, the finite-difference time-domain (FDTD) method is applied to calculate the radar cross-section (RCS) of anisotropic coated missiles. We present a FDTD algorithm for cylindrical coordinates and derive the necessary extension to the FDTD equations for a general three-dimensional anisotropic scatterer. A new approach is proposed to obtain magnitude and phase information from the FDTD data. Computed results for two selected examples are compared with those obtained by eigenfunction expansion techniques and the moment method (MM) to demonstrate the validity of the new approach with very good agreement. The study of the bistatic radar cross-section for a missile demonstrates that the anisotropic material coating around it can effectively reduce its RCS.

## 1. INTRODUCTION

The basic FDTD method in Cartesian coordinates, first described by Yee [1], has been used extensively in electromagnetic field modeling because of its ability to robustly handle interactions of fields with complex heterogeneous structures. The method can also handle materials characterized by arbitrary permittivity, conductivity and permeability including anisotropic media [2]. A study of electromagnetic scattering from a conducting target, having an dielectric layer over it, is a field of great interest to engineering

community [3–5]. In using the conventional FDTD algorithm to solve such electromagnetic scattering problems involving curved surfaces, which are poorly represented in a rectilinear mesh, the traditional rectangular cells to such surfaces results in the staircase approximation. Generalizing the FDTD algorithm to curvilinear coordinates [6, 7] can obviously improve the accuracy of the model. For the current problem discussed in this paper, the conventional FDTD algorithm should be modified to accommodate anisotropic materials in cylindrical coordinates. In addition, a conformal dielectric FDTD technique [8] is useful for the accurate description of arbitrary shaped surfaces.

## 2. METHODOLOGY

Maxwell's time-domain curl equations in an isotropic, homogeneous and lossy dielectric medium have the form

$$\nabla \times \boldsymbol{E} = -\mu \frac{\partial \boldsymbol{H}}{\partial t} \qquad \nabla \times \boldsymbol{H} = \varepsilon \frac{\partial \boldsymbol{E}}{\partial t} + \sigma \boldsymbol{E} \tag{1}$$

where $\boldsymbol{E}$ is the electric field intensity, $\boldsymbol{H}$ is the magnetic field intensity, $\varepsilon$ is the dielectric constant, $\mu$ is the permeability and $\sigma$ is the conductivity.

In a cylindrical coordinate system $(\rho, \varphi, z)$, it is assumed that the space-time functional notation $f^n(i, j, k) = f(i\Delta\rho, j\Delta\varphi, k\Delta z, n\Delta t)$ applies, where $\Delta\rho$ and $\Delta z$ are the respective space increments along the $\rho$- and $Z$-directions, $\Delta\varphi$ is the angular increment along the azimuthal direction, and $\Delta t$ is the time increment. Following Yee [1], both the temporal and spatial derivatives in the scalar equations of Eq. (1) are approximated by central difference expressions that have second-order accuracy in the space and time increments, and the resulting update equations for $\boldsymbol{E}$ can be represented as

$$\begin{aligned} E_\rho^{n+1}(i+\frac{1}{2}, j, k) = {} & E_\rho^n(i+\frac{1}{2}, j, k) + \frac{\Delta t}{\varepsilon_0(i+\frac{1}{2})\Delta\rho\Delta\varphi} \\ & \cdot \left[ Hz^{n+\frac{1}{2}}(i+\frac{1}{2}, j+\frac{1}{2}, k) - Hz^{n+\frac{1}{2}}(i+\frac{1}{2}, j-\frac{1}{2}, k) \right] \\ & - \frac{\Delta t}{\varepsilon_0 \Delta z} \left[ H_\varphi^{n+\frac{1}{2}}(i+\frac{1}{2}, j, k+\frac{1}{2}) - H_\varphi^{n+\frac{1}{2}}(i+\frac{1}{2}, j, k-\frac{1}{2}) \right] \end{aligned} \tag{2a}$$

$$\begin{aligned} E_\varphi^{n+1}(i, j+\frac{1}{2}, k) = {} & E_\varphi^n(i, j+\frac{1}{2}, k) + \frac{\Delta t}{\varepsilon_0 \Delta z} \\ & \cdot \left[ H_\rho^{n+\frac{1}{2}}(i, j+\frac{1}{2}, k+\frac{1}{2}) - H_\rho^{n+\frac{1}{2}}(i, j+\frac{1}{2}, k-\frac{1}{2}) \right] \end{aligned}$$

$$-\frac{\Delta t}{\varepsilon_0 \Delta\rho}\left[H_z^{n+\frac{1}{2}}(i+\frac{1}{2},j+\frac{1}{2},k)-H_z^{n+\frac{1}{2}}(i-\frac{1}{2},j+\frac{1}{2},k)\right] \tag{2b}$$

$$\begin{aligned} E_z^{n+1}(i,j,k+\frac{1}{2}) &= E_z^n(i,j,k+\frac{1}{2}) + \frac{\Delta t}{\varepsilon_0 i\Delta\rho} \\ &\cdot\left[(i+\frac{1}{2})H_\varphi^{n+\frac{1}{2}}(i+\frac{1}{2},j,k+\frac{1}{2})-(i-\frac{1}{2})H_\varphi^{n+\frac{1}{2}}(i-\frac{1}{2},j,k+\frac{1}{2})\right] \\ &-\frac{\Delta t}{\varepsilon_0 i\Delta\rho\Delta\varphi}\left[H_\rho^{n+\frac{1}{2}}(i,j+\frac{1}{2},k+\frac{1}{2})-H_\rho^{n+\frac{1}{2}}(i,j-\frac{1}{2},k+\frac{1}{2})\right]. \end{aligned} \tag{2c}$$

Similar time-stepping equations can be obtained for the magnetic field components.

The following relations hold in general anisotropic material

$$\boldsymbol{D} = \varepsilon_0 \boldsymbol{\varepsilon}_r \cdot \boldsymbol{E}, \quad \boldsymbol{B} = \mu_0 \boldsymbol{\mu}_r \cdot \boldsymbol{H}, \quad \boldsymbol{J} = \boldsymbol{\sigma} \cdot \boldsymbol{E} \tag{3}$$

where $\boldsymbol{D}$ is the electric displacement vector, $\boldsymbol{B}$ is the magnetic induction vector, $\boldsymbol{\varepsilon}_r$ is the relative permittivity tensor, $\boldsymbol{\mu}_r$ is the relative permeability tensor, and $\boldsymbol{\sigma}$ is the conductivity tensor, which can be written as

$$\boldsymbol{\varepsilon}_r = \begin{bmatrix} \varepsilon_{\rho\rho} & \varepsilon_{\rho\varphi} & \varepsilon_{\rho z} \\ \varepsilon_{\varphi\rho} & \varepsilon_{\varphi\varphi} & \varepsilon_{\varphi z} \\ \varepsilon_{z\rho} & \varepsilon_{z\varphi} & \varepsilon_{zz} \end{bmatrix}, \ \boldsymbol{\mu}_r = \begin{bmatrix} \mu_{\rho\rho} & \mu_{\rho\varphi} & \mu_{\rho z} \\ \mu_{\varphi\rho} & \mu_{\varphi\varphi} & \mu_{\varphi z} \\ \mu_{z\rho} & \mu_{z\varphi} & \mu_{zz} \end{bmatrix}, \ \boldsymbol{\sigma} = \begin{bmatrix} \sigma_{\rho\rho} & \sigma_{\rho\varphi} & \sigma_{\rho z} \\ \sigma_{\varphi\rho} & \sigma_{\varphi\varphi} & \sigma_{\varphi z} \\ \sigma_{z\rho} & \sigma_{z\varphi} & \sigma_{zz} \end{bmatrix} \tag{4}$$

We assume these off-diagonal elements are nonzero. Following Schneider and Hudson [2], we obtain

$$E_{\rho_{i+\frac{1}{2},j,k}}^{n+1} = [W_{11} \ \ W_{12} \ \ W_{13}] \cdot (\boldsymbol{Q} \cdot \boldsymbol{N}_1 - \boldsymbol{M}_1) \tag{5a}$$

$$E_{\varphi_{i,j+\frac{1}{2},k}}^{n+1} = [W_{21} \ \ W_{22} \ \ W_{23}] \cdot (\boldsymbol{Q} \cdot \boldsymbol{N}_2 - \boldsymbol{M}_2) \tag{5b}$$

$$E_{z_{i,j,k+\frac{1}{2}}}^{n+1} = [W_{31} \ \ W_{32} \ \ W_{33}] \cdot (\boldsymbol{Q} \cdot \boldsymbol{N}_3 - \boldsymbol{M}_3) \tag{5c}$$

The tensors $\boldsymbol{W}$ and $\boldsymbol{Q}$ take the form

$$\boldsymbol{W} = \begin{bmatrix} W_{11} & W_{12} & W_{13} \\ W_{21} & W_{22} & W_{23} \\ W_{31} & W_{32} & W_{33} \end{bmatrix} = \begin{bmatrix} \frac{\varepsilon_{\rho\rho}}{\Delta t}+\frac{\sigma_{\rho\rho}}{2} & \frac{\varepsilon_{\rho\varphi}}{\Delta t}+\frac{\sigma_{\rho\varphi}}{2} & \frac{\varepsilon_{\rho z}}{\Delta t}+\frac{\sigma_{\rho z}}{2} \\ \frac{\varepsilon_{\varphi\rho}}{\Delta t}+\frac{\sigma_{\varphi\rho}}{2} & \frac{\varepsilon_{\varphi\varphi}}{\Delta t}+\frac{\sigma_{\varphi\varphi}}{2} & \frac{\varepsilon_{\varphi z}}{\Delta t}+\frac{\sigma_{\varphi z}}{2} \\ \frac{\varepsilon_{z\rho}}{\Delta t}+\frac{\sigma_{z\rho}}{2} & \frac{\varepsilon_{z\varphi}}{\Delta t}+\frac{\sigma_{z\varphi}}{2} & \frac{\varepsilon_{zz}}{\Delta t}+\frac{\sigma_{zz}}{2} \end{bmatrix}^{-1}$$

$$\boldsymbol{Q}=\begin{bmatrix} Q_{11} & Q_{12} & Q_{13} \\ Q_{21} & Q_{22} & Q_{23} \\ Q_{31} & Q_{32} & Q_{33} \end{bmatrix}=\begin{bmatrix} \frac{\varepsilon_{\rho\rho}}{\Delta t}-\frac{\sigma_{\rho\rho}}{2} & \frac{\varepsilon_{\rho\varphi}}{\Delta t}-\frac{\sigma_{\rho\varphi}}{2} & \frac{\varepsilon_{\rho z}}{\Delta t}-\frac{\sigma_{\rho z}}{2} \\ \frac{\varepsilon_{\varphi\rho}}{\Delta t}-\frac{\sigma_{\varphi\rho}}{2} & \frac{\varepsilon_{\varphi\varphi}}{\Delta t}-\frac{\sigma_{\varphi\varphi}}{2} & \frac{\varepsilon_{\varphi z}}{\Delta t}-\frac{\sigma_{\varphi z}}{2} \\ \frac{\varepsilon_{z\rho}}{\Delta t}-\frac{\sigma_{z\rho}}{2} & \frac{\varepsilon_{z\varphi}}{\Delta t}-\frac{\sigma_{z\varphi}}{2} & \frac{\varepsilon_{zz}}{\Delta t}-\frac{\sigma_{zz}}{2} \end{bmatrix}$$

where the superscript $-1$ indicates inverting the corresponding matrix. We will limit ourselves here to consideration of the vectors $\boldsymbol{N}_1$ and $\boldsymbol{M}_1$ in the first relation in Eq. (5).

$$\boldsymbol{N}_1=\begin{bmatrix} E^n_{\rho_{i+\frac{1}{2},j,k}} \\ \frac{1}{4}\left(E^n_{\varphi_{i+1,j+\frac{1}{2},k}}+E^n_{\varphi_{i+1,j-\frac{1}{2},k}}+E^n_{\varphi_{i,j+\frac{1}{2},k}}+E^n_{\varphi_{i,j-\frac{1}{2},k}}\right) \\ \frac{1}{4}\left(E^n_{z_{i+1,j,k+\frac{1}{2}}}+E^n_{z_{i+1,j,k-\frac{1}{2}}}+E^n_{z_{i,j,k+\frac{1}{2}}}+E^n_{z_{i,j,k-\frac{1}{2}}}\right) \end{bmatrix}$$

$$\boldsymbol{M}_1=\begin{bmatrix} \frac{\partial H_z^{n+\frac{1}{2}}}{\rho\partial\varphi}-\frac{\partial H_\varphi^{n+\frac{1}{2}}}{\partial z} \\ \frac{\partial H_\rho^{n+\frac{1}{2}}}{\partial z}-\frac{\partial H_z^{n+\frac{1}{2}}}{\partial\rho} \\ \frac{\partial(\rho H_\varphi^{n+\frac{1}{2}})}{\rho\partial\rho}-\frac{\partial H_\rho^{n+\frac{1}{2}}}{\rho\partial\varphi} \end{bmatrix} \tag{6}$$

Where

$$\begin{aligned}\frac{\partial H_\rho^{n+\frac{1}{2}}}{\rho\partial\varphi} &= \frac{1}{4(i+\frac{1}{2})\Delta\rho\Delta\varphi}\Big[H^{n+\frac{1}{2}}_{\rho_{i+1,j+\frac{1}{2},k+\frac{1}{2}}}+H^{n+\frac{1}{2}}_{\rho_{i+1,j+\frac{1}{2},k-\frac{1}{2}}}+H^{n+\frac{1}{2}}_{\rho_{i,j+\frac{1}{2},k+\frac{1}{2}}} \\ &\quad -H^{n+\frac{1}{2}}_{\rho_{i,j+\frac{1}{2},k-\frac{1}{2}}}-H^{n+\frac{1}{2}}_{\rho_{i+1,j-\frac{1}{2},k+\frac{1}{2}}}-H^{n+\frac{1}{2}}_{\rho_{i+1,j-\frac{1}{2},k-\frac{1}{2}}} \\ &\quad -H^{n+\frac{1}{2}}_{\rho_{i+1,j-\frac{1}{2},k+\frac{1}{2}}}-H^{n+\frac{1}{2}}_{\rho_{i+1,j-\frac{1}{2},k-\frac{1}{2}}}\Big] \end{aligned} \tag{7a}$$

$$\begin{aligned}\frac{\partial(\rho H_\varphi^{n+\frac{1}{2}})}{\rho\partial\rho} &= \frac{1}{4\Delta\rho}\Big[H^{n+\frac{1}{2}}_{\varphi_{i+\frac{3}{2},j,k+\frac{1}{2}}}+H^{n+\frac{1}{2}}_{\varphi_{i+\frac{3}{2},j,k-\frac{1}{2}}}-H^{n+\frac{1}{2}}_{\varphi_{i-\frac{1}{2},j,k+\frac{1}{2}}}-H^{n+\frac{1}{2}}_{\varphi_{i-\frac{1}{2},j,k-\frac{1}{2}}} \\ &\quad \cdot\frac{1}{4(i+\frac{1}{2})\Delta\rho}\Big[H^{n+\frac{1}{2}}_{\varphi_{i+\frac{3}{2},j,k+\frac{1}{2}}}+H^{n+\frac{1}{2}}_{\varphi_{i+\frac{3}{2},j,k-\frac{1}{2}}}+H^{n+\frac{1}{2}}_{\varphi_{i-\frac{1}{2},j,k+\frac{1}{2}}} \\ &\quad +H^{n+\frac{1}{2}}_{\varphi_{i-\frac{1}{2},j,j,k-\frac{1}{2}}}\Big] \end{aligned} \tag{7b}$$

$$\frac{\partial H_\rho^{n+\frac{1}{2}}}{\partial z} = \frac{1}{4\Delta z}\Big[H^{n+\frac{1}{2}}_{\rho_{i+1,j+\frac{1}{2},k+\frac{1}{2}}}+H^{n+\frac{1}{2}}_{\rho_{i+1,j-\frac{1}{2},k+\frac{1}{2}}}+H^{n+\frac{1}{2}}_{\rho_{i,j+\frac{1}{2},k+\frac{1}{2}}}$$

$$
\begin{aligned}
&-H^{n+\frac{1}{2}}_{\rho_{i,j-\frac{1}{2},k+\frac{1}{2}}} - H^{n+\frac{1}{2}}_{\rho_{i+1,j+\frac{1}{2},k-\frac{1}{2}}} - H^{n+\frac{1}{2}}_{\rho_{i+1,j-\frac{1}{2},k-\frac{1}{2}}} \\
&- H^{n+\frac{1}{2}}_{\rho_{i+1,j+\frac{1}{2},k-\frac{1}{2}}} - H^{n+\frac{1}{2}}_{\rho_{i+1,j-\frac{1}{2},k-\frac{1}{2}}}\Bigg] \qquad (7c)
\end{aligned}
$$

$$
\begin{aligned}
\frac{\partial H_z^{n+\frac{1}{2}}}{\partial \rho} &= \frac{1}{4\Delta\rho}\Bigg[H^{n+\frac{1}{2}}_{z_{i+\frac{3}{2},j,k+\frac{1}{2}}} + H^{n+\frac{1}{2}}_{z_{i+\frac{3}{2},j,k-\frac{1}{2}}} \\
&\quad - H^{n+\frac{1}{2}}_{z_{i-\frac{1}{2},j,k+\frac{1}{2}}} - H^{n+\frac{1}{2}}_{z_{i-\frac{1}{2},j,k-\frac{1}{2}}}\Bigg] \qquad (7d)
\end{aligned}
$$

$$
\frac{\partial H_\varphi^{n+\frac{1}{2}}}{\partial z} = \frac{1}{\Delta z}\left[H^{n+\frac{1}{2}}_{\varphi_{i+\frac{1}{2},j,k+\frac{1}{2}}} - H^{n+\frac{1}{2}}_{\varphi_{i+\frac{1}{2},j,k-\frac{1}{2}}}\right] \qquad (7e)
$$

$$
\frac{\partial H_z^{n+\frac{1}{2}}}{\rho\partial \varphi} = \frac{1}{(i+\frac{1}{2})\Delta\rho\Delta\varphi}\left[H^{n+\frac{1}{2}}_{z_{i+\frac{1}{2},j+\frac{1}{2},k}} - H^{n+\frac{1}{2}}_{z_{i+\frac{1}{2},j-\frac{1}{2},k}}\right] \qquad (7f)
$$

It is considerably different from the isotropic media cases that four terms of $\boldsymbol{N}_1$ depend upon $E_y$ or $E_z$ neighboring $E_x$, and there is additionally the derivative with respect to $x$ in the expressions of $\boldsymbol{M}_1$. In calculating the remaining electric field components, similar procedures must be carried out for deriving the equations of $\boldsymbol{N}_2, \boldsymbol{M}_2, \boldsymbol{N}_3$, and $\boldsymbol{M}_3$. Using the same scheme, we can obtain the FDTD equations for the magnetic field in anisotropic media having a permeability tensor.

In order to model open-region problems, an absorbing boundary condition is often used to truncate the computational domain, and ensures that this boundary is, in effect, transparent to outgoing waves. Although absorbing performance of the standing-traveling wave boundary condition [9] is not particularly good as widely used PML (perfectly matched layer), it is easier to handle, and requires smaller CPU storage without additional absorbing domain and fields splitting. In addition, it is independent of incident frequency and angle, and can be extended to dispersive or lossy media. In 3-D cylindrical coordinates, this boundary consists of the cylinder surface $\rho = N_\rho\Delta\rho$, the planes $Z = 0$ and $Z = N_z\Delta z$. The STWBC are expressed as follows:

$$
\begin{aligned}
E_\rho^{n+1}(i+\frac{1}{2},j,0) = 0.5\Bigg\{&E_\rho^n(i+\frac{1}{2},j,0) + \frac{\Delta t}{\varepsilon_0(i+\frac{1}{2})\Delta\rho\Delta\varphi} \\
&\cdot\left[H_z^{n+\frac{1}{2}}(i+\frac{1}{2},j+\frac{1}{2},0) - H_z^{n+\frac{1}{2}}(i+\frac{1}{2},j-\frac{1}{2},0)\right] \\
&- \frac{2\Delta t}{\varepsilon_0\Delta z}H_\varphi^{n+\frac{1}{2}}(i+\frac{1}{2},j,\frac{1}{2})\Bigg\} \qquad (8a)
\end{aligned}
$$

$$E_{\varphi}^{n+1}(i,j+\frac{1}{2},0) = 0.5\left\{E_{\varphi}^{n}(i,j+\frac{1}{2},0) + \frac{2\Delta t}{\varepsilon_0\Delta z}H_{\rho}^{n+\frac{1}{2}}(i,j+\frac{1}{2},\frac{1}{2}) - \frac{\Delta t}{\varepsilon_0\Delta\rho}\left[H_z^{n+\frac{1}{2}}(i+\frac{1}{2},j+\frac{1}{2},0) - H_z^{n+0.5}(i-\frac{1}{2},j+\frac{1}{2},0)\right]\right\} \tag{8b}$$

$$E_{\rho}^{n+1}(i+\frac{1}{2},j,N_z) = 0.5\left\{E_{\rho}^{n}(i+\frac{1}{2},j,N_z) + \frac{\Delta t}{\varepsilon_0(i+\frac{1}{2})\Delta\rho\Delta\varphi} \cdot\left[H_z^{n+\frac{1}{2}}(i+\frac{1}{2},j+\frac{1}{2},N_z) - H_z^{n-\frac{1}{2}}(i+\frac{1}{2},j-\frac{1}{2},N_z)\right] + \frac{2\Delta t}{\varepsilon_0\Delta z}H_{\varphi}^{n+\frac{1}{2}}(i+\frac{1}{2},j,N_z-\frac{1}{2})\right\} \tag{8c}$$

$$E_{\varphi}^{n+1}(i,j+\frac{1}{2},N_z) = 0.5\left\{E_{\varphi}^{n}(i,j+\frac{1}{2},N_z) - \frac{2\Delta t}{\varepsilon_0\Delta z}H_{\rho}^{n+\frac{1}{2}}(i,j+\frac{1}{2},N_z-\frac{1}{2}) - \frac{\Delta t}{\varepsilon_0\Delta\rho}\left[H_z^{n+\frac{1}{2}}(i+\frac{1}{2},j+\frac{1}{2},N_z) - H_z^{n+\frac{1}{2}}(i-\frac{1}{2},j+\frac{1}{2},N_z)\right]\right\} \tag{8d}$$

$$E_{\varphi}^{n+1}(N_\rho,j+\frac{1}{2},k) = 0.5\left\{E_{\varphi}^{n}(N_\rho,j+\frac{1}{2},k) + \frac{\Delta t}{\varepsilon_0\Delta z} \cdot\left[H_{\rho}^{n+\frac{1}{2}}(N_\rho,j+\frac{1}{2},k+\frac{1}{2}) - H_{\rho}^{n+\frac{1}{2}}(N_\rho,j+\frac{1}{2},k-\frac{1}{2})\right] + \frac{2\Delta t}{\varepsilon_0\Delta\rho}H_z^{n+\frac{1}{2}}(N_\rho-\frac{1}{2},j+\frac{1}{2},k)\right\} \tag{8e}$$

$$E_{z}^{n+1}(N_\rho,j,k+\frac{1}{2}) = E_{z}^{n}(N_\rho,j,k+\frac{1}{2}) - \frac{2\Delta t}{\varepsilon_0 N_\rho\Delta\rho}(i-\frac{1}{2}) \cdot H_{\varphi}^{n+\frac{1}{2}}(i-\frac{1}{2},j,k+\frac{1}{2}) - \frac{\Delta t}{\varepsilon_0 N_\rho\Delta\rho\Delta\varphi} \cdot\left[H_{\rho}^{n+\frac{1}{2}}(N_\rho,j+\frac{1}{2},k+\frac{1}{2}) - H_{\rho}^{n+\frac{1}{2}}(N_\rho,j-\frac{1}{2},k+\frac{1}{2})\right] \tag{8f}$$

$$E_{\varphi}^{n+1}(N_\rho,j+\frac{1}{2},0) = 0.5\left\{E_{\varphi}^{n}(N_\rho,j+\frac{1}{2},0) + \frac{2\Delta t}{\varepsilon_0\Delta z} H_{\rho}^{n+\frac{1}{2}}(N_\rho,j+\frac{1}{2},\frac{1}{2}) + \frac{2\Delta t}{\varepsilon_0\Delta\rho}H_z^{n+\frac{1}{2}}(N_\rho-\frac{1}{2},j+\frac{1}{2},0)\right\} \tag{8g}$$

$$E_{\varphi}^{n+1}(N_\rho, j+\frac{1}{2}, N_z) = 0.5\left\{E_{\varphi}^{n}(N_\rho, j+\frac{1}{2}, N_z) - \frac{2\Delta t}{\varepsilon_0 \Delta z} \cdot H_{\rho}^{n+\frac{1}{2}}(N_\rho, j+\frac{1}{2}, N_z-\frac{1}{2}) + \frac{2\Delta t}{\varepsilon_0 \Delta \rho} H_{z}^{n+\frac{1}{2}}(N_\rho-\frac{1}{2}, j+\frac{1}{2}, N_z)\right\} \quad (8h)$$

Cylindrical coordinate system has singularities along the $z$-axis. Cells adjacent to this line are formed of only five sides instead of six, and the field components $H_\rho, E_Y$ and $E_z$ updates for these cells require special attention. The former two field components are not required for the update equations of any other components, so they are simply ignored by the algorithm. From the Ampere's law, we obtain

$$E_z^{n+1}(0, j, k+\frac{1}{2}) = E_z^n(0, j, k+\frac{1}{2}) + \sum_j \frac{2\Delta t}{\varepsilon_0 \pi \Delta \rho} H_{\varphi}^{n+\frac{1}{2}}(\frac{1}{2}, j, k) \quad (9)$$

We assume that $N_Y$ is the total mesh number in azimuthal direction, namely, the azimuthal index $j \in [0, N_Y]$. Thus, the FDTD equations for $E_\rho$ $(j=0)$, $E_z$ $(j=0)$, $H_\rho$ $(j=N_Y-\frac{1}{2})$ and $H_z$ $(j=N_Y-\frac{1}{2})$ must be modified as

$$E_{\rho}^{n+1}(i+\frac{1}{2}, 0, k) = E_{\rho}^{n}(i+\frac{1}{2}, 0, k) + \frac{\Delta t}{\varepsilon_0 (i+\frac{1}{2}) \Delta\rho\Delta\varphi} \cdot \left[H_z^{n+\frac{1}{2}}(i+\frac{1}{2}, \frac{1}{2}, k) - H_z^{n+\frac{1}{2}}(i+\frac{1}{2}, N_\varphi-\frac{1}{2}, k)\right] - \frac{\Delta t}{\varepsilon_0 \Delta z}\left[H_{\varphi}^{n+\frac{1}{2}}(i+\frac{1}{2}, 0, k+\frac{1}{2}) - H_{\varphi}^{n+\frac{1}{2}}(i+\frac{1}{2}, 0, k-\frac{1}{2})\right] \quad (10a)$$

$$E_z^{n+1}(i, 0, k+\frac{1}{2}) = E_z^n(i, 0, k+\frac{1}{2}) + \frac{\Delta t}{\varepsilon_0 i \Delta\rho}\left[(i+\frac{1}{2}) H_{\varphi}^{n+\frac{1}{2}}(i+\frac{1}{2}, 0, k+\frac{1}{2}) - (i-\frac{1}{2}) H_{\varphi}^{n+\frac{1}{2}}(i-\frac{1}{2}, 0, k+\frac{1}{2})\right] - \frac{\Delta t}{\varepsilon_0 i \Delta\rho\Delta\varphi}\left[H_{\rho}^{n+\frac{1}{2}}(i, \frac{1}{2}, k+\frac{1}{2}) - H_{\rho}^{n+\frac{1}{2}}(i, N_\varphi-\frac{1}{2}, k+\frac{1}{2})\right] \quad (10b)$$

$$H_{\rho}^{n+\frac{1}{2}}(i, N_\varphi-\frac{1}{2}, k+\frac{1}{2}) = H_{\rho}^{n-\frac{1}{2}}(i, N_\varphi-\frac{1}{2}, k+\frac{1}{2}) + \frac{\Delta t}{\mu_0 i \Delta\rho\Delta\varphi} \cdot \left[Ez^n(i, 0, k+\frac{1}{2}) - Ez^n(i, N_\varphi-1, k+\frac{1}{2})\right] - \frac{\Delta t}{\mu_0 \Delta z}\left[E_{\varphi}^{n}(i, N_\varphi-\frac{1}{2}, k+1) - E_{\varphi}^{n}(i, N_\varphi-\frac{1}{2}, k)\right] \quad (10c)$$

$$H_z^{n+\frac{1}{2}}(i+\frac{1}{2},N_\varphi-\frac{1}{2},k)=H_z^{n-\frac{1}{2}}(i+\frac{1}{2},N_\varphi-\frac{1}{2},k)-\frac{\Delta t}{\mu_0(i+\frac{1}{2})\Delta\rho}$$
$$\cdot\left[(i+\frac{1}{2})E_\varphi^n(i+1,N_\varphi-\frac{1}{2},k)-(i-\frac{1}{2})E_\varphi^n(i,N_\varphi-\frac{1}{2},k)\right]$$
$$+\frac{dt}{\mu_0(i+\frac{1}{2})\Delta\rho\Delta\varphi}\left[E_\rho^n(i+\frac{1}{2},0,k)-E_\rho^n(i+\frac{1}{2},N_\varphi-1,k)\right] \quad (10d)$$

To transform the near scattered field to the far field, magnitude and phase information for sinusoidal steady-state FDTD problems can be obtained by the undermentioned approach. The time-harmonic electromagnetic field having the following form:

$$f(t)=f_0\cos(\omega t+\phi) \quad (11)$$

where all variables are real numbers, and $f_0$ is the magnitude and $\phi$ is the initial phase. Then the derivative of $f(t)$ is

$$\frac{df(t)}{dt}=-\omega f_0\sin(\omega t+\phi) \quad (12)$$

and it is approximated by the difference quotient expression as

$$\frac{f(t+\Delta t)-f(t)}{\Delta t}=-\omega f_0\sin(\omega t+\phi) \quad (13)$$

where $\Delta t$ is still the time step. Obviously $\Delta t$ is far smaller than the one in Cartesian coordinates, so the discretization error is very small. Using (12) and (13), one can obtain the magnitude and the phase from the FDTD data at time step $n$ and $n+1$.

## 3. NUMERICAL RESULTS

In order to validate the feasibility of the current FDTD algorithm to analyze electromagnetic scattering, canonical two-dimensional structures are studied. The numerical results of the FDTD-computed surface electric-current distribution are presented for the cases of a two-dimensional conducting circular cylinder and a dielectrically coated conducting cylinder respectively subject to a TE-polarized illumination at normal incidence.

The perfectly conducting circular cylinder excited by an external transverse electric plane wave of unit amplitude whose propagation vector and electric polarization vector are, respectively, perpendicular and parallel to the axis of the cylinder as shown in Fig. 1. The wavelength $\lambda$ is chosen to make $k_0a=5$, where $k_0$, $a$ are the

propagation constant in the free-space medium, and the radius of the cylinder. Fig. 1 graphs the results for the FDTD analyses of the magnitude and phase of the cylinder surface-current distribution. A plane wave of unit amplitude traveling along $X$-axis is incident on a circular conducting cylinder coated with homogenous dielectric layer as shown in Fig. 2. The ratio of $a$ to $\lambda$ is 0.4, and the thickness of the dielectric coating $\delta = 0.06\lambda$. The relative dielectric constant $\varepsilon_r = 2.0$.

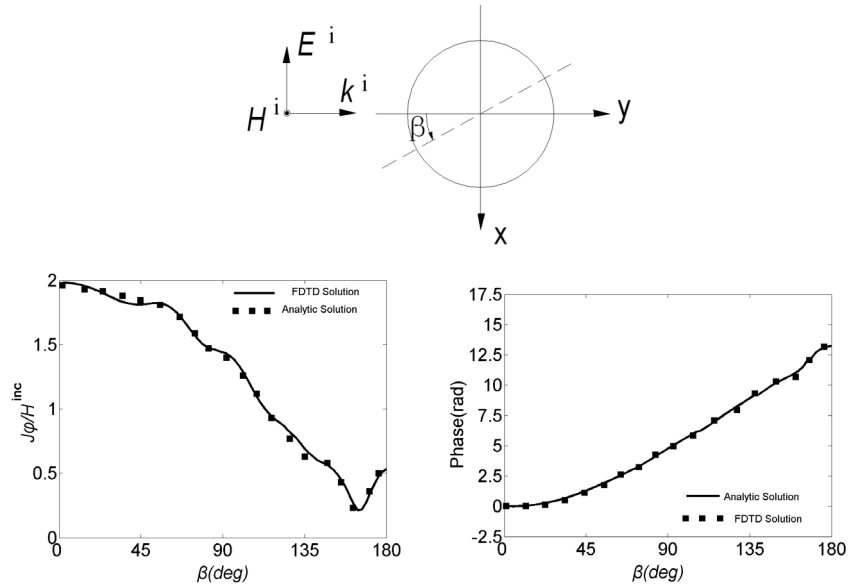


**Figure 1.** Magnitude and phase of electric current on the circular cylinder surface.

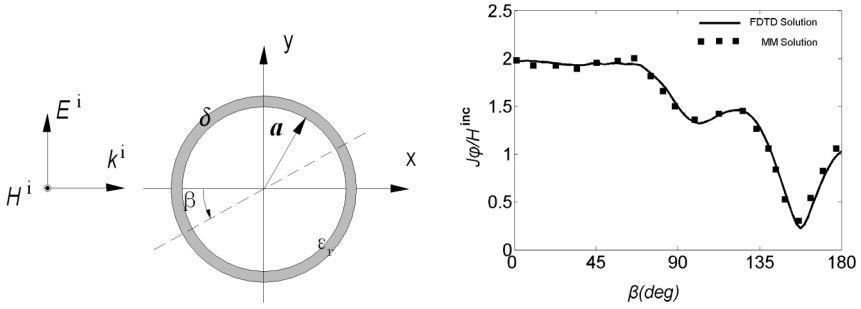


**Figure 2.** Magnitude of electric current on the inner cylinder.

The magnitude of the inner cylinder surface-current distribution is shown in Fig. 2. These results are in excellent agreement with those obtained by eigenfunction expansion techniques [6] and the moment method (MM) [10].

The photograph of a real antitank missile is contained in Fig. 3(1). In the light of the geometrical configuration of the missile, a model is constructed as shown in Fig. 3(2). The nose of the model points along the $z$-axis, and its two horizontal fins lie in the $XZ$ plane, the vertical one lies in the $YZ$ plane. The missile model consists of a conical nose and a cylinder; three fins are mounted in the midst of the fuselage. We take the fins to be wedge-shaped, and the angle of each fin to the axis of the missile is 18°. The constitutive parameters of the model are: $a = 20.8\,\text{cm}$, $b = 138.6\,\text{cm}$, $c = 48.5\,\text{cm}$, $d = 69\,\text{cm}$, $e = 24\,\text{cm}$, $f = 12\,\text{cm}$, whose graphical definitions are given in Fig. 3(2). The electromagnetic parameters of the anisotropic coating are: $\varepsilon_\rho = 10$, $\varepsilon_\varphi = 30$, $\varepsilon_z = 70$, $\mu = 20$, $\sigma = 0.07$, and its thickness is 4 mm. The incident wave whose electric field vector is parallel to the $X$-axis propagates along $-z$ direction with the frequency 300 MHz.

In the bistatic cases, the transmitter and receiver will be confined to the horizontal plane, namely $XZ$ plane. The bistatic scattering cross-section for both the bare case and the coated case of the missile model is calculated. Fig. 4 plots the cross-section of the missile as a function of the bistatic angle $\beta$ and shows the effect of the coating layer on the monostatic scattering cross-section. It is seen that the anisotropic material coating around the missile can evidently reduce its RCS.

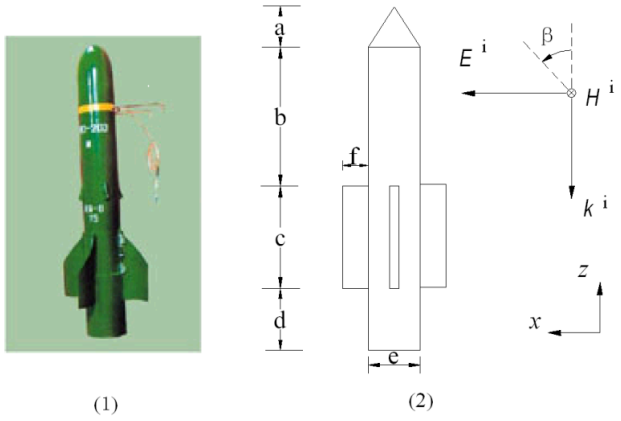


**Figure 3.** (1) Photograph of a real antitank missile (2) Geometry of a missile model scattering problem.

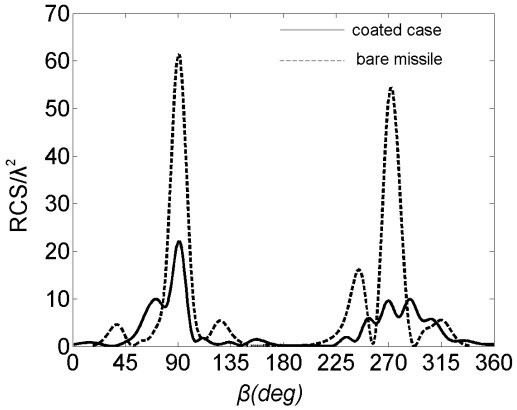


**Figure 4.** Effect of coating on scattering cross-section.

## 4. CONCLUSIONS

We have extended the FDTD algorithm in cylindrical coordinates to accommodate anisotropic materials with general permittivity, conductivity and permeability tensors, which cannot be diagonalized. Two validating examples have been reported representing excellent accuracy of the current method. The results for both bare and coated case of a missile demonstrate the effect of the anisotropic material coating around it on its RCS reduction.

## REFERENCES

1. Yee, K. S., "Numerical solution of initial boundary value problems involving Maxwell's equations in isotropic media," *IEEE Trans. AP*, Vol. 14, No. 4, 302–307, 1966.
2. Schneider, J. and S. Hudson, "The finite-difference time-domain method applied to anisotropic material," *IEEE Trans. AP*, Vol. 41, No. 7, 994–999, 1993.
3. Zheng, H. X., X. Q. Sheng, and E. K. N. Yung, "Computation of scattering from anisotropically coated bodies using conformal FDTD," *Progress In Electromagnetics Research*, PIER 35, 287–297, 2002.
4. Shim, J. and H. T. Kim, "Dominance of creeping wave modes of backscattered field from a conducting sphere with dielectric coating," *Progress In Electromagnetics Research*, PIER 21, 293–306, 1999.

5. Li, L. W., T. S. Yeo, and M. S. Leong, "Bistatic scattering and backscattering of electromagnetic waves by conducting and coated dielectric spheroids: a new analysis using mathematica package," *Progress In Electromagnetics Research*, PIER 31, 225–245, 2001.
6. Fusco, M. A., "FDTD algorithm in curvilinear coordinates," *IEEE Trans. on AP*, Vol. 38, No. 1, 76–89, 1990.
7. Fusco, M. A., M. V. Smith, and L. W. Gordon, "A three-dimensional FDTD algorithm in curvilinear coordinates," *IEEE Trans. AP*, Vol. 39, No. 10, 1463–1471, 1991.
8. Yu, W. H. and R. Mittra, "A conformal finite difference time domain technique for modeling curved dielectric surfaces," *IEEE Microwave and Wireless Components Letters*, Vol. 11, No. 1, January 2001.
9. Tan, H. Y., K. Liu, and D. Liang, "Standing-traveling wave boundary condition (STWBC) for finite-difference time-domain mesh truncation," *IEE Electronics Letters*, Vol. 36, No. 6, 408–409, 2000.
10. Lin, C. S. and M. T. Yaqoob, "A moment solution for scattering from a dielectrically coated conducting cylinder," *IEEE AP-S, Digest*, Vol. 2, 777–780, Jul. 18–25, 1992.